Cell Reports Medicine, Volume *2*

Supplemental information

Compromised mitochondrial quality control triggers lipin1-related rhabdomyolysis

Yamina Hamel, François-Xavier Mauvais, Marine Madrange, Perrine Renard, Corinne Lebreton, Ivan Nemazanyy, Olivier Pellé, Nicolas Goudin, Xiaoyun Tang, Mathieu P. Rodero, Caroline Tuchmann-Durand, Patrick Nusbaum, David N. Brindley, Peter van Endert, and Pascale de Lonlay

SUPPLEMENTAL INFORMATION

Figures S1–5

Table S1

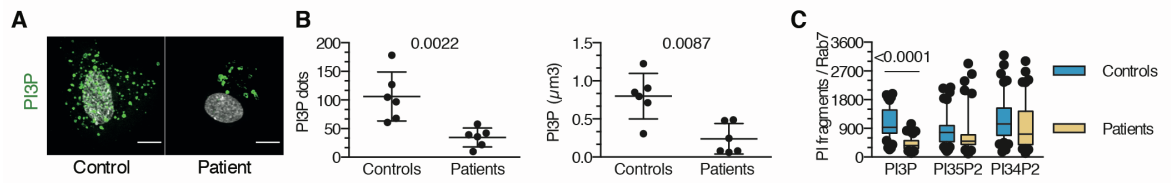

Figure S1. Number, size and distribution of PI fragments. **Related to Figure 2**. **(A)** Myoblasts from control individuals and patients were immunostained to detect the endogenous PI3P phospholipid. Images show a representative staining for 1 out of 6 control individuals and 1 out of 6 patients. Scale bars, 10 µm. **(B)** The dot plots (30 images/dot) represents the mean ± SD number of PI3P vesicles *(left)* and mean ± SD volume (Mann-Whitney U-test) determined with the Imaris software *(right)* in control and patient myoblasts. **(C)** The box and whiskers plots (50 images/condition) show the median, 10^{th} percentile and 90^{th} percentile number of PI3P, PI34P2 and PI35P2 fragments contained among a binary mask created to define the Rab7 surface in the myoblasts of 1 out of 3 patients and controls. The images are from 1 out of at least 3 independent experiments.

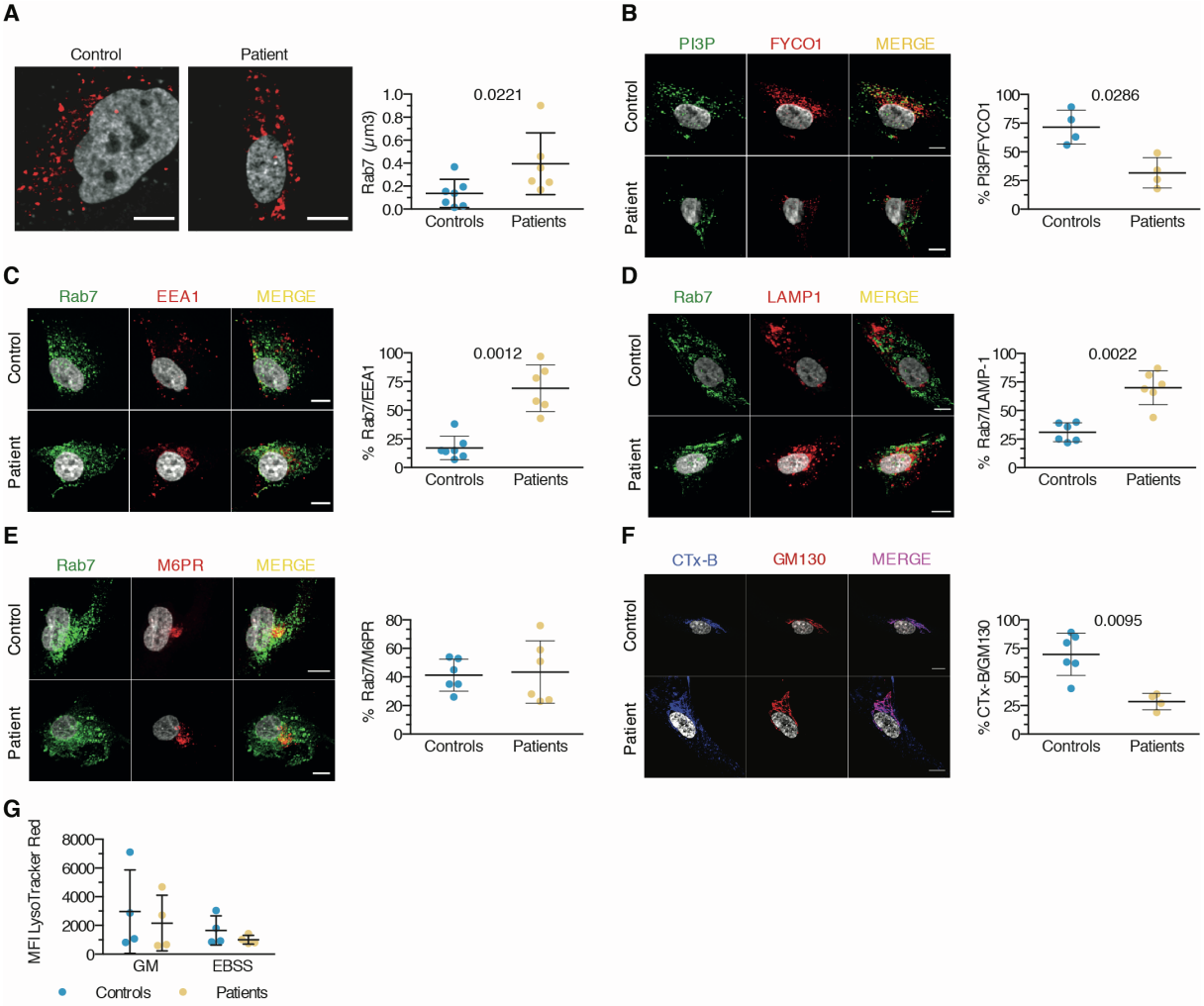

Figure S2. Lipin1 regulates late endosome maturation and functions. Related to Figure 3. (A) The images show a focus on perinuclear Rab7 vesicles observed by confocal microscopy after staining with a specific antibody, from 1 out of 6 control individuals and patients. Imaris software was used to segment these vesicles and determine their volume. The dot plot shows the mean ± SD (mean of 50 images/dot) volume of $Rab7^{+}$ vesicles in control and patient myoblasts. **(B)** A representative confocal image of myoblasts from 1 out of 4 controls and patients immunostained with PI3P and FYCO1 is shown. The dot plots (mean of 50 image/dot) represent the mean ± SD percentage of proximity of PI3P with FYCO1 (Mann-Whitney U-test). **(C-E)** As in **(A),** but evaluating the proximity of Rab7 with EEA1 **(C)**, Rab7 with M6PR **(D)** or Rab7 with LAMP1 **(E)** in myoblasts of 6 controls and patients (mean of 30-40 images/dot). **(F)** Cholera toxin B (CTx-B) retrograde transport was monitored by confocal microscopy. The dot plots (mean of 30 images/dot) represent the mean ± SD percentage of proximity of CTx-B with the GM130 Golgi marker (Mann-Whitney U-test). **(G)** Myoblasts from 4 control individuals and 4 patients cultured with a nutrient-rich growth medium (GM) or a starvation medium (EBSS) were loaded with the fluorescent LysoTracker Deep Red™ probe before processing for flow cytometry. Dot plots depict the mean ± SD of mean fluorescence intensity (MFI) of LysoTracker Red (mean effect of interaction $F(1,12)=0.00684$, $p=0.9355$, of stimulus $F(1,12)=1.83$, $p=0.2011$, of subjects $F(1,12)=0.629$, $p=0.4433$; between-subjects two-way ANOVA). Scale bars, 10 µm **(A-F)**. Results are from 1 out of at least 3 independent experiments.

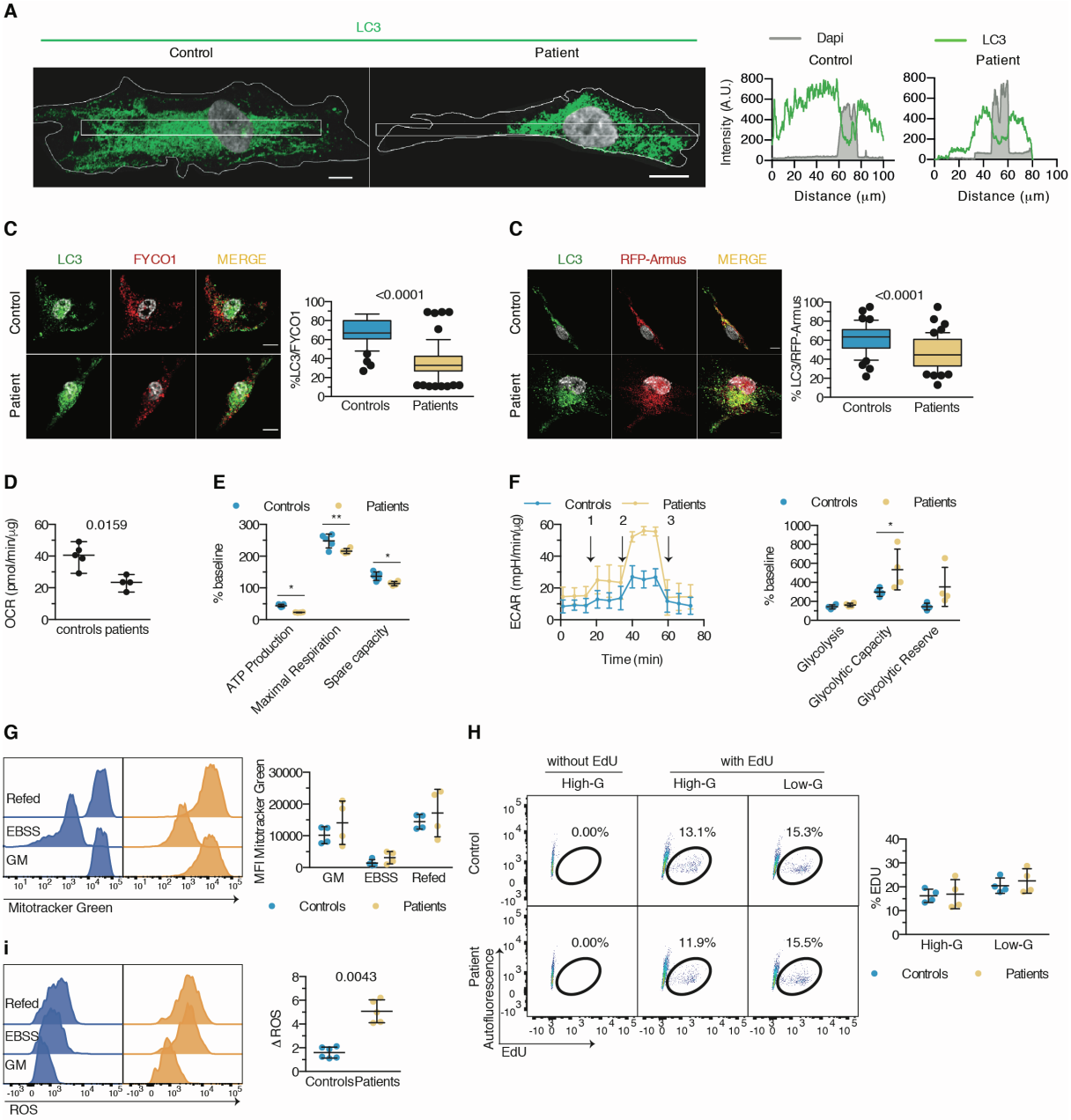

Figure S3. Lipin1 regulates autophagosome positioning and functions and mitochondrial functions. Related to Figure 4. (A) The distribution of endogenous LC3 in control and patient myoblasts was determined by calculating the intensity of LC3 fluorescence along a longitudinal axis traversing the nucleus of 30 individual cells per condition. The graph illustrates the perinuclear accumulation of LC3 marker in control vs patient cells. Images and graphs are representative of 1 out of 4 patients and control individuals. **(B)** Myoblasts were exposed to EBSS and immunostained to detect LC3 and FYCO1 by confocal microscopy. The images show the co-staining from 1 out of 2 controls and patients. Box and whiskers dot plots (mean of 80 images/condition) shows the median, 10th percentile and 90th percentile of the percentage of proximity of LC3 with FYCO1 (Mann-Whitney U-test). **(C)** Myoblasts transfected with a plasmid construct encoding for Armus-RFP were immunostained to detect LC3 and the proximity between the 2 proteins was quantified (unpaired t-test) and depicted into box and whiskers plots as in **(B). (D),** As in **Figure 4 (D)** but dot plots (mean of 4 technical replicates/dot) depict mean ± SD of the Oxidative Consumption Rate (OCR) at baseline (Mann-Whitney U-test). **(E)** As in **Figure 4 (D)** but dot plots depict the relative proportion of ATP production, maximal respiration capacity and spare capacity after normalization to basal respiration (baseline), in 5 patients and 5 control individuals (mean effect of interaction F(2,14)=0.7049, p=0.5109, of time F(2,14)=899.8, p<0.0001, of subjects F(1,7)=17.90, p=0.0039; within-subjects two-way ANOVA). **(F)** *left:* Dot plot with lines show the mean ± SD ECAR production over time and after addition of glucose (1), oligomycin (2) and 2-desoxyglucose (3) by the myoblasts from 4 controls and patients; *right:* dot plot (mean of 4 technical values/dot) depicts the mean ± SD of the relative proportion of glycolysis, glycolytic capacity and glycolytic reserve after normalization to basal production (mean effect of interaction F(2,12)=3.129, p=0.0806, of time F(2,12)=16.10, p=0.0004, of subjects F(1,6)=5.07, p=0.0652; within-subjects two-way ANOVA). **(G)** FACS plots represent the mitochondrial mass of myoblasts from 1 out of 4 patients and control individuals loaded with the MitoTracker Green dye and exposed to EBSS and refed (Refed) or not with a nutrient-rich medium (GM). Dot plots represent the mean ± SD of the MFI or MitoTracker Green (mean effect of interaction F(2,18)=0.1205, p=0.8871, of stimulus F(2,18)=19.72, p<0.0001, of subjects F(1,18)=2.312, p=0.1458; between-subjects two-way ANOVA). **(H)** Myoblasts from 4 patients and control individuals were cultured in a low-glucose (low-G) concentration vs high-glucose (high-G) concentration nutrient-rich growth medium for 3 days then loaded with EdU, fixed, permeabilized and processed for flow cytometry. FACS plots represent data from 1 out of 4 controls and patients. Dot plots (mean of 2 technical replicates) show the mean ± SD percentage of EdU incorporated in myoblasts form controls and patients (mean effect of interaction F(1,12)=0.08935, p=0.7701, of stimulus F(1,12)=4.709, p=0.0508, of subjects F(1,12)=0.3443, p=0.5682; between-subjects two-way ANOVA). **(I)** As in **(G)** but ROS production was evaluated by flow

cytometry performed on myoblasts from 6 patients and control individuals. Dot plots show the mean ± SD of the MFI of cells exposed to EBSS normalized to the MFI of cells exposed to GM (Mann-Whitney U-test). Scale bars, 10 μm. *, $p<0.05$, **, $p<0.01$, ***, $p<0.001$, ****, $p<0.0001$: adjusted p-values as determined by two-way ANOVA and post-hoc Sidak's correction. Results are from 1 out of at least 3 independent experiments.

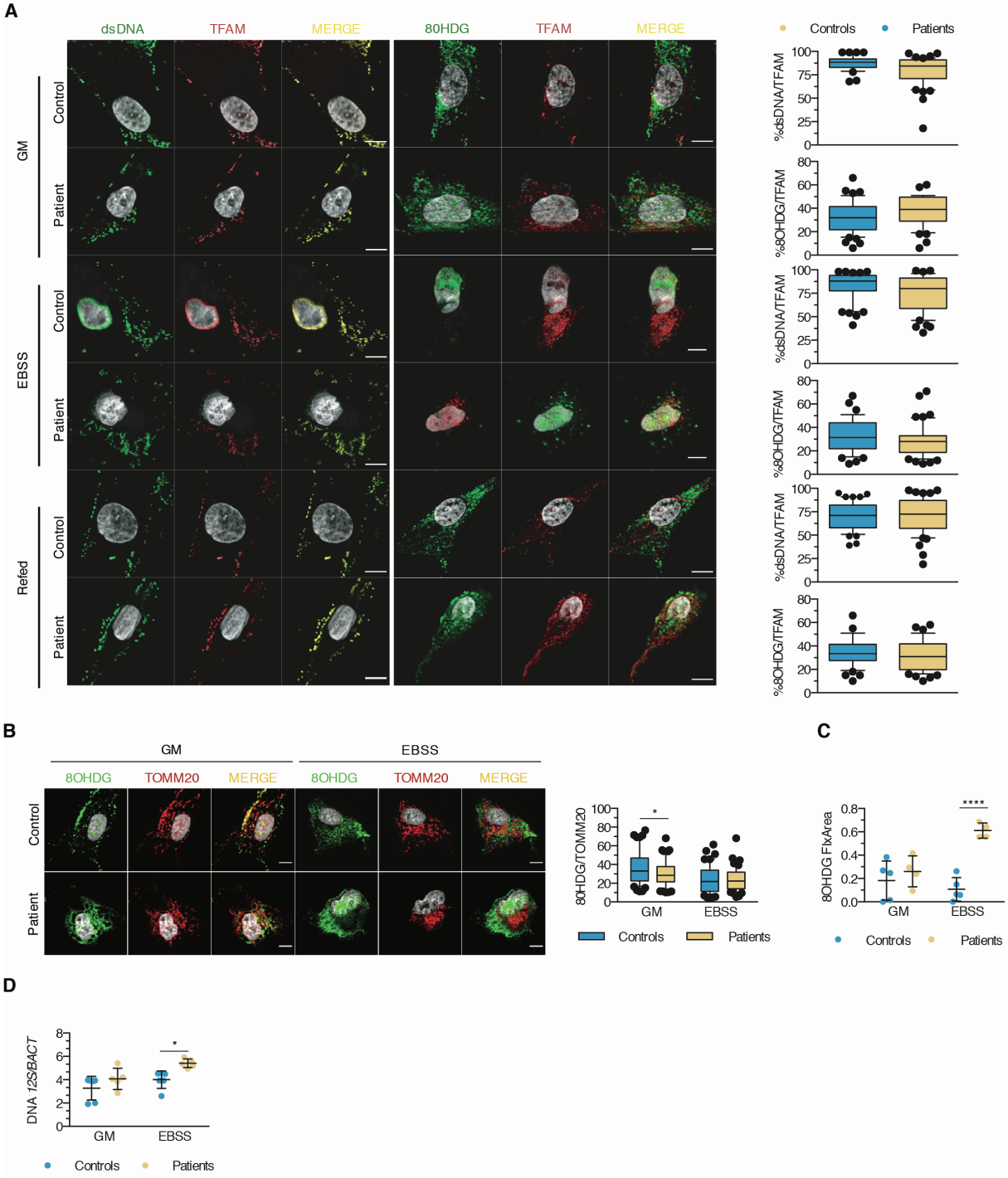

Figure S4. Oxidized mtDNA accumulate into autophagosomes and late endosomes/lysosomes in the absence of lipin1. Related to Figure 4. (A) Myoblasts exposed to EBSS and refed (Refed) with a nutrient-rich growth medium (GM) were processed for confocal imaging and stained with anti-dsDNA or anti-8OHDG (green) and anti-TFAM (red) antibodies. Box and whisker plots (mean of 50 images/condition) show the median, 10th percentile and 90th percentile of the percentage of proximity of dsDNA or 8OHDG with TFAM (not significant, Mann-Whitney U-test). Images and graphs show the results of 1 out of 2 patients and control individuals. **(B)**Accumulation of damaged mitochondria was evaluated by co-staining myoblasts with anti-8OHDG and anti-TOMM20 antibodies following exposure to EBSS or nutrient-rich GM. Box and whiskers plots (50 images/condition) display the median, 10th percentile and 90th percentile of proximity of 8OHDG with TOMM20 (mean effect of interaction F(1,196)=2.312, p=0.1300, of stimulus F(1,196)=21.70, p<0.0001, of subjects F(1,196)=2.865, P=0.0921; between-subjects two-way ANOVA). Images and graphs show the results of 1 out of 3 patients and control individuals. **(C)** Accumulation of oxidized mtDNA following exposure to EBSS was quantified as anti-8OHDG fluorescence intensity (FI) per cell pixel area (FI x Area) analyzed. Dot plots (mean of 30 images/dot) show the mean ± SD of 8OHDG FI x Area in myoblasts of 4 controls and patients (mean effect of interaction F(1,14)=12.74, p=0.0031, of stimulus F(1,14)=5.333, p=0.0367, of subjects F(1,14)=23.98, p=0.0002; between-subjects two-way ANOVA). **(D)** Dot plots (mean of 3 technical replicates/dot) show the mean ± SD relative level of *12S* mtDNA content normalized to genomic *BACT* DNA in myoblasts from 3 controls and 3 patients exposed to nutrient-rich GM or EBSS, as quantified by qPCR (mean effect of interaction F(1,18)=0.7487, p=0.3983, of stimulus F(1,18)=8.712, p=0.0085, of subjects F(1,18)=9.928, p=0.0055; between-subjects two-way ANOVA). Scale bars, 10 µm (**A, B**). *, p<0.05, **, p<0.01, ***, p<0.001, ****, p<0.0001 as determined by two-way ANOVA and post-hoc Sidak's correction for multiple comparisons. The results are from 1 representative out of 2 **(A, B)** or 3 **(C, D)** independent experiments.

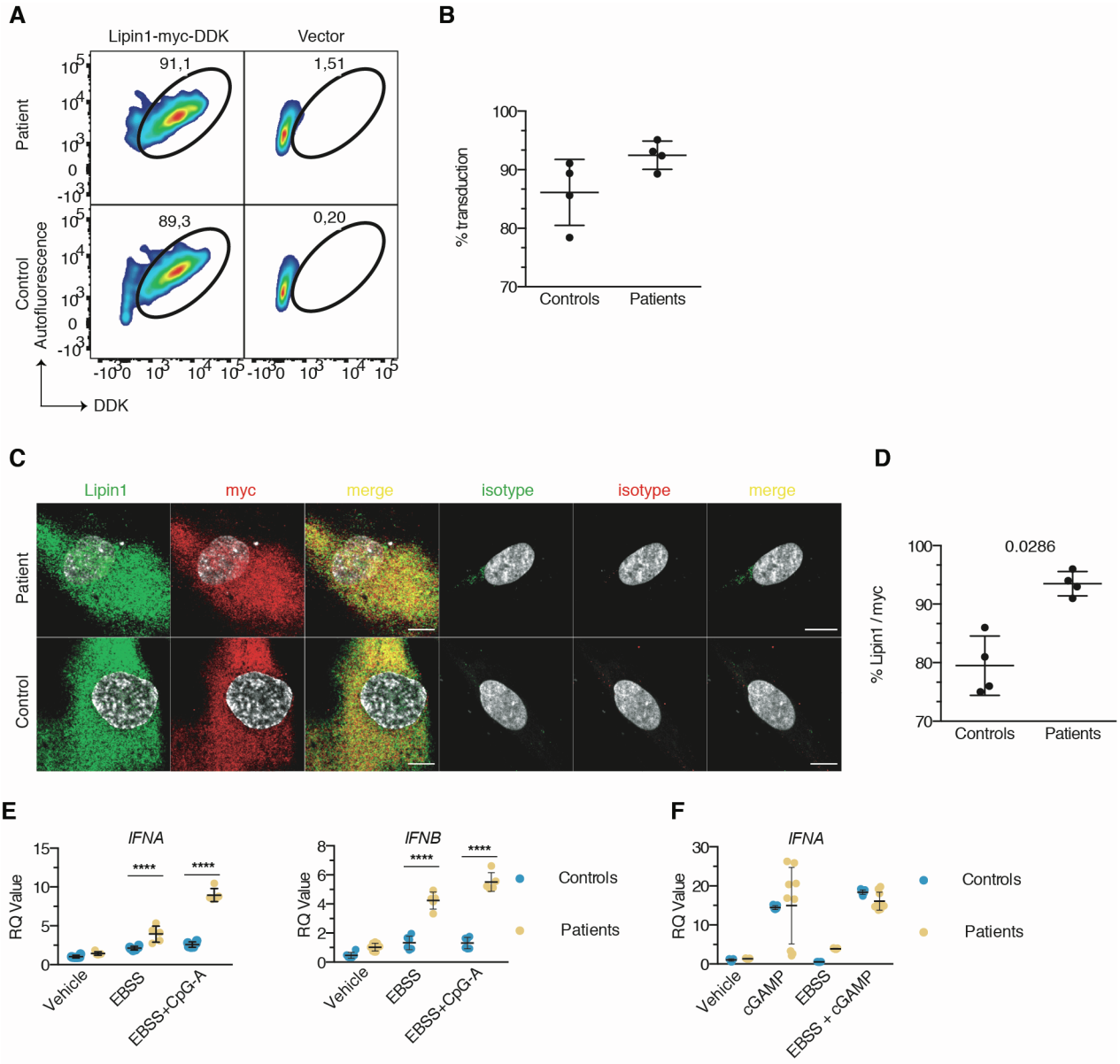

Figure S5. Oxidized mtDNA preferentially activates TLR9-dependent inflammation in lipin1-deficient myoblasts. Related to Figure 5. (A) Myoblasts from 4 patients and 4 control individuals were transduced with a lentivirus expressing a plasmid encoding for myc-DDK-tagged lipin1 protein or an empty vector. FACS plots (>1,000 single cells) depict the expression of DDK in cells fixed, permeabilized and stained with a specific antibody. **(B),** Dot plot show the mean ± SD percentage of transduction in 4 controls and 4 patients (not significant, Mann-Whitney U-test) determined by flow cytometry as in **(A)**. **(C)** As in **(A)** and **(B)**, but cells were stained for lipin1 and myc tag protein using specific antibodies or isotypic controls before processing for confocal microscopy. The images are from 1 out of 4 controls and patients. Scale bars, 10 µm. **(D),** As in **(C)**, but dot plot (30-40 cells/condition) represents the mean ± SD percentage of proximity of lipin1 with myc tag protein in 4 patients and 4 control individuals (Mann-Whitney U-test). **(E),** Dot plot (mean of 3 technical replicates/dot) depicts the mean ± SD *IFNA* expression normalized to *BACT* expression measured by qPCR in myoblasts of 6 controls and patients (mean effect of interaction F(3,64)=1.929, p=0.1337, of stimulus F(3,64 =97.74, p<0.0001, of subjects F(1,64)=0.3235, p=0.5715; between-subjects two-way ANOVA) upon stimulation with the STING-activating ligand cGAMP performed either in rich-nutrient GM or EBSS. **(F)** Myoblasts from 6 control individuals and patients were exposed to EBSS and challenged or not with CpG-A. Dot plots (mean of 3 technical replicates) show the mean ± SD of *IFNA* (left panel; mean effect of interaction F(2,27)=85.06, p< 0.0001, of stimulus F(2,27)=181.2, p<0.0001, of subjects F(1,27)=214.8, p<0.0001; two-way ANOVA) and *IFNB* (right panel; mean effect of interaction F(2,31)=59.92, p<0.0001, of stimulus F(2,31)=137.7 ,p<0.0001, of subjects F(1,31)=321.4, p<0.0001) normalized *to BACT* levels by qPCR. Results are representative from 1 out of 2 (**D**) or 3 (**A-C, E**) independent experiments. *, p<0.05, **, p<0.01, ***, p<0.001, ****, p<0.0001: adjusted p-values as determined by two-way ANOVA and post-hoc Sidak's correction.

Table S1. Clinical and molecular characteristics of patients with *LPIN1* mutations. Related to STAR Methods.

Patient	Gender	Age at onset (years)	Age at diagnosis (years)	Number of severe RM (CK> 10, 000 U/L), main trigger	Mutations (NM_145693.4)	Mutated residues	Figure panels
P1	M	2	5	7, fever	c.1162C>T c.1162C>T	p.Arg388* p.Arg388*	1A-C, 2A, 2C-D, 3A-E, 5A-K, 6A-C, 6D-F, 6H-I, S1A-C, S2A, S2C-G, S3A, S3C-I, S5A-F
P2	M	5	10	3, fever	c.1162C>T c.1162C>T	p.Arg388* p.Arg388*	1A-C, 2A, 3A, 3F-I, 4A-B, 5A, 5C, 5E, 5I, S1A, S2A-G, S3D-E, S3I, S4B-C, S5E-F
P3	M	5	7	1, fever	c.1441+2T>C c.2295-866_2410-30del		1A-C, 2A, 3A-I, 5A-K, 6A-C, 6D-F, 6H-I, S1A, S2A-F, S3A-I, S4C-D, S5A-F
P4	M	14	12	1, fever	c.1441+2T>C c.2295-866_2410-30del		1A-C, 2A, 2C-D, 3A, 4A-B, 5A, 5C-E, 5H-I, S1A-C, S2A, S2C-G, S3D-I, S4A-D, S5E-F
P5	F	3	3	3, gastroenteritis	c.1441+2T>C c.2295-866_2410-30del		1A-C, 2A, 3A-G, 5A-C, 5E-I, 6A-C, 6D-F, 6H-I, S1A, S2A-G, S3A-C, S3I, S5A-F
P6	F	2	2	4, gastroenteritis	c.2295-863_2410-27del c.2295-863_2410-27del	p.Glu766_Ser838del p.Glu766_Ser838del	1A, 2A, 2C-D, 3A, 3G-I, 4A-B, 5A-K, 6A-C, 6D-F, 6H-I, S1A-C, S2A-F, S3A, S3D-I, S4A-D, S5A-F

M: Male; F: Female; RM: Rhabdomyolysis.